DOI 10.7343/as-2026-959

ACQUE SOTTERRANEE
Italian Journal of Groundwater
journal homepage: https://www.acquesotterranee.net/

Ensemble Space Inversion (ENSI) yields efficient and realistic calibration of a multi-layer volcanic aquifer model

Ensemble Space Inversion (ENSI) per una calibrazione efficiente e realistica di un modello di acquifero vulcanico multistrato

Mattia De Caro[a], Licia Pollicino[a], Giovanni Formentin[a]

a - HPC Italia S.r.l., email: *Mattia.Decaro@hpc.ag; Licia.Pollicino@hpc.ag; Giovanni.Formentin@hpc.ag*

ARTICLE INFO

Ricevuto/*Received*: 7 January 2026
Accettato/*Accepted*: 17 June 2026
Pubblicato online/*Published online*: 30 June 2026

Handling Editor:
Wondimagegn Abebe Demissie

Editor in Chief:
Iacopo Borsi

Citation:
De Caro, M., Pollicino, L., Formentin, G. (2026). Ensemble Space Inversion (ENSI) yields efficient and realistic calibration of a multi-layer volcanic aquifer model
Acque Sotterranee - *Italian Journal of Groundwater*, 15(2), 51 - 62
https://doi.org/10.7343/as-2026-959

Correspondence to:
Mattia De Caro
Mattia.Decaro@hpc.ag

Keywords: *Ensemble Space Inversion, PEST, high-dimensional inverse problem, volcanic multi-aquifer system, model calibration, parameter uncertainty.*

Parole chiave: Ensemble Space Inversion, PEST, problema inverso ad altà dimensionalità, acquifero vulcanico, calibrazione inversa, incertezza dei parametri.

Abstract

Calibration (history-matching) of groundwater flow and transport models is an essential step to minimize posterior predicting uncertainty, enabling their use to design interventions such as remediation systems in contaminated sites. To encapsulate all information coming from field observations, especially in complex hydrogeological settings, hight dimensional inverse problems are usually set up, which may be difficult or very lengthy to solve. This study applies the Ensemble Space Inversion (ENSI) method to a multi-layer groundwater flow model developed using MODFLOW-USG to design a hydraulic barrier in an industrial area in Central Italy. ENSI projects the inversion problem into a reduced-dimensional parameter space using super-parameters derived from stochastic realizations. The method yields a fast solution that preserves geological plausibility where standard history-matching tools fail to even reach convergence. Results show excellent agreement between observed and simulated heads and drawdowns, with significant computational savings compared to traditional approaches. ENSI proves to be a robust and practical tool for complex hydrogeological models, especially in data-rich and highly heterogeneous settings.

Riassunto

La calibrazione (*history-matching*) dei modelli di flusso e trasporto in falda rappresenta una fase essenziale per minimizzare l'incertezza predittiva a posteriori, consentendo il loro impiego nella progettazione di interventi quali i sistemi di bonifica nei siti contaminati. Per integrare tutte le informazioni provenienti dalle osservazioni di campo, soprattutto in contesti idrogeologici complessi, solitamente vengono implementati problemi inversi ad alta dimensionalità, la cui risoluzione può risultare difficile o estremamente onerosa. Questo studio applica il metodo Ensemble Space Inversion (ENSI) ad un modello di flusso sotterraneo multi-acquifero, sviluppato con MODFLOW-USG al fine di progettare una barriera idraulica in un'area industriale dell'Italia centrale. ENSI proietta il problema inverso in uno spazio dei parametri a dimensione ridotta utilizzando super-parametri derivanti da realizzazioni stocastiche. Il metodo consente di ottenere una soluzione rapida che preserva la plausibilità geologica, anche nei casi in cui gli strumenti tradizionali di calibrazione non riescono a raggiungere la convergenza. I risultati mostrano un'eccellente corrispondenza tra livelli piezometrici e abbassamenti osservati e simulati, con un significativo risparmio computazionale rispetto agli approcci convenzionali. ENSI si dimostra quindi uno strumento robusto e pratico per modelli idrogeologici complessi, in particolare in contesti ricchi di dati e caratterizzati da elevata eterogeneità.

Introduction

In the context of contaminated aquifer management, groundwater flow modeling is widely recognized as an essential decision-support tool for addressing some environmental issues, such as the design and optimization of pollutant containment measures and the prediction of aquifer responses under different management scenarios (Anderson et al., 2015).

To assimilate information contained in the available data, a thorough calibration process is required. Model calibration is the procedure through which model parameters are adjusted to achieve an optimal fit between model outputs and field measurements (Moore & Doherty, 2006). It follows that the concept of calibration infers parameter uniqueness, even in problems where the number of unknown parameters, representing the hydraulic properties of a heterogeneous and complex hydrogeological system, may exceed the information content of the available observations, rendering the problem an "ill-posed" inverse problem (Doherty & Hunt, 2010) – which is, in fact, the case with almost all real world applications. As a result, a unique "best-fit" parameter set is just a sampling out of an infinite set of combinations: as such, it provides an incomplete representation of the real system and leads to wrong model predictions.

To address this issue, modern calibration approaches often incorporate regularization, ensemble-based methods, and uncertainty quantification to explore the range of plausible parameter sets and improve confidence in predictive outcomes (Tonkin & Doherty, 2009). A significant enhancement in model calibration was the introduction of the PEST (Parameter ESTimation) software suite (Doherty, 2003), which offers advanced regularization techniques, including Tikhonov regularization and Singular Value Decomposition (SVD) approaches, to stabilize parameter estimation in highly parameterized models (Doherty & Hunt, 2010). While iteratively minimizing the discrepancies between observations and their simulated counterparts, PEST can apply regularization to constrain the parameter solution space, preventing extreme or physically unrealistic values and ensuring spatial or conceptual consistency in distributed parameter fields (Doherty & Hunt, 2010). In addition, SVD identifies parameter combinations that are most influential on model outputs, reducing the dimensionality of optimization problems, improving numerical stability, and mitigating the non-uniqueness commonly encountered in highly parameterized inversions.

Notwithstanding the benefits of regularization and SVD methods, the standard application of the Gauss-Levenberg-Marquardt algorithm (GLM) can impose a prohibitive computational burden on highly parameterized calibration problems (Fienen et al., 2009). The burden mainly comes from the necessity to populate the so-called Jacobian matrix containing sensitivities of all observations to parameters, which implies at least a forward model per parameter at each PEST iteration. To overcome this limitation, ensemble-based methods are increasingly being adopted in hydrogeology. These approaches simplify both the calibration process and uncertainty analysis through an ensemble of model realizations, allowing parameter–observation relationships to be inferred statistically rather than through repeated full Jacobian calculations (Chen & Oliver, 2013). Among these, the Iterative Ensemble Smoother (iES), Data-Space Inversion (DSI) and Ensemble-Space Inversion (ENSI) methodologies have been applied across a range of complex hydrogeological calibration problems, demonstrating their computational and practical effectiveness (Kitlasten et al., 2025; Delottier et al., 2023). The iES technique provides efficient parameter estimates by progressively incorporating observation data into an ensemble of model realizations, rather than relying on traditional gradient-based optimization (Hayley et al., 2019). The DSI method performs the inversion directly in the space of observations, avoiding explicit parameter-space adjustments (Mariethoz et al., 2010; Sun & Durlofsky, 2017; Lima et al., 2020; Liu et al., 2021). The ENSI approach projects the calibration problem into a reduced ensemble subspace derived from an ensemble of model realizations. Observations are assimilated into the ensemble to adjust the super-parameters-low-dimensional linear combinations of the native model parameter fields that span the principal directions of model sensitivity. The optimized super-parameters are then used to reconstruct the full-resolution native parameter fields (hydraulic conductivity, storage coefficients, etc.) via back-projection onto the ensemble subspace (Doherty, 2021). Recent comparative assessments have demonstrated the effectiveness of ENSI and related ensemble-based approaches across a range of complex hydrogeological calibration problems (Kitlasten et al., 2025; Delottier et al., 2023).

In this study, the ENSI method has been tested in conjunction with PEST_HP (Doherty, 2024) to calibrate a multi-layer groundwater flow model representing a complex volcanic multi-aquifer system in Central Italy, to be applied for the configuration of hydraulic barriers. The model has been implemented under both steady-state and transient conditions with the aim of reproducing field observations collected during some pumping tests. Over 1,900 head and drawdown measurements were used as observation datasets to constrain the parameter estimation process, which incorporated 480 pilot points, resulting in a highly parameterized optimization problem.

The specific objectives of this study are: (i) to implement and test the ENSI methodology in a complex, high-dimensional volcanic multi-aquifer system representing a real contaminated site; (ii) to evaluate ENSI calibration performance against a large observational dataset comprising over 1,900 hydraulic head and drawdown measurements collected during 13 pumping tests; (iii) to discuss both the advantages and limitations of the ENSI approach relative to conventional parameter estimation methods.

Materials and methods

Study area

The study area, located in an undisclosed location in Central Italy, is characterized by a complex stratigraphic succession composed of pyroclastic products, lava flows, sandy and lapilli layers (Fig. 1). The alluvial deposits forming the uppermost sequence consist predominantly of fine silty-clayey sediments with interbedded sandy layers of variable thickness. Beneath these deposits, the subsoil is made up of massive and chaotic pozzolanic and tuff layers. Tuff deposits are generally lithified but locally may exhibit intense fracturing. They separate the pozzolanic deposits into two different layers: an upper one and a lower one. While upper pozzolanic deposits are typically incoherent, with a color ranging from brown to brown-orange, lower pozzolanic deposits are usually black in color, semi-coherent, with a cineritic-scoraceous matrix containing dispersed black leucite-bearing scoria. The upper portions of the deep pozzolanic deposits are characterized by the presence of paleosols, whose thickness is difficult to determine due to insufficient stratigraphic information. The deposits underlying this massive pyroclastic succession consist of lava layers with variable degrees of fracturing.

From the hydrogeological point of view, shallow alluvial deposits are predominantly unsaturated or host only a perched water table disconnected from the deeper aquifer system hosted within the underlying volcanic succession. This volcanic sequence exhibits high heterogeneity, both in terms of hydrodynamic parameters and mechanisms of vertical groundwater flow. The presence of paleosols, which can act as aquitard, confining the deeper saturated layers, together with the high variability in the thickness of the tuff layer and the different degrees of fracturing that characterize the volcanic deposits account for extremely complex groundwater flow dynamics.

In the study area, two main aquifers have been identified: an intermediate aquifer, hosted in tuff deposits, and a deep aquifer, hosted in the lower pozzolanic and lava layers, confined by the overlying paleosols. Results from recent pumping tests have revealed that the intermediate aquifer is characterized by low values of both hydraulic conductivity (ranging from 10^{-6} to 10^{-5} m/s) and transmissivity (ranging from 10^{-5} to 10^{-4} m^2/s), whereas the deep aquifer shows high values of both hydraulic conductivity (usually higher than 10^{-4} m/s) and transmissivity (ranging from 10^{-3} to 10^{-2} m^2/s). These parameter ranges are derived from pumping tests conducted at the site during the environmental characterization phase. The values are consistent with those reported in the literature for tuff-hosted and pozzolanic aquifer systems in comparable volcanic settings (Custodio & Llamas, 1983; Civita & De Maio, 2000).

The volcanic sequence is emplaced in a tectonically active extensional setting, a context common to many volcanic districts of central Italy, where normal faulting can create sub-vertical structural discontinuities. Such discontinuities may act as either conduits or barriers to groundwater flow, potentially influencing vertical connectivity between the intermediate and deep aquifer units. In the study area, direct evidence of fault-controlled inter-aquifer communication was not identified during site investigations; however, this possibility was considered in the conceptual model and is implicitly represented in the numerical model through the spatially variable vertical hydraulic conductivity of the paleosol layer. This parameterization allows localized drainage pathways potentially associated with structural heterogeneities to be accounted for in groundwater flow modelling.

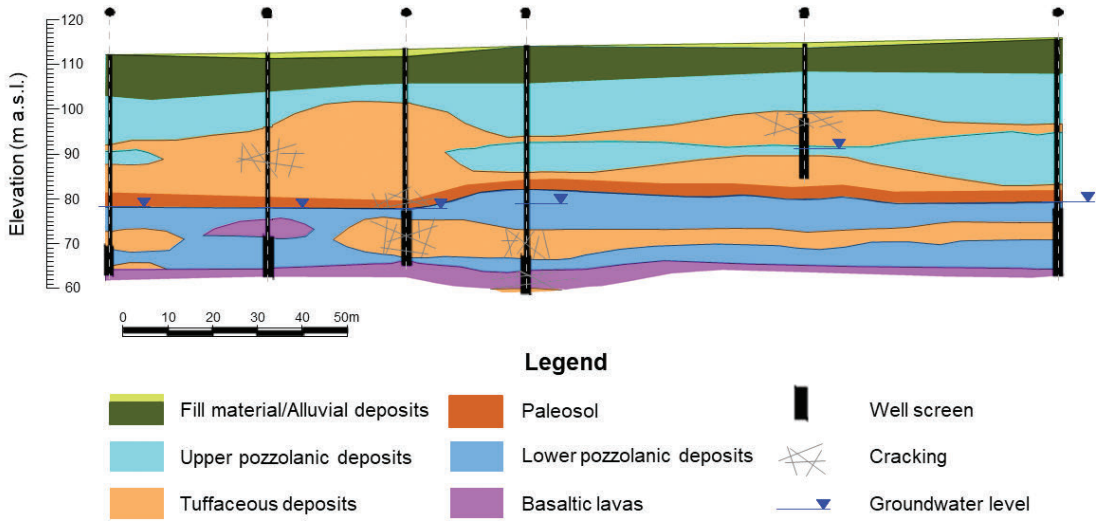

Fig. 1 - Conceptual stratigraphic cross-section of the study area illustrating the major hydro-stratigraphic units. Variations in layer thickness, pinch-outs, and interfingering of units highlight the complex depositional environment controlling groundwater flow. Monitoring wells shown along the cross-section indicate screened intervals and groundwater level measurements used for model calibration. Fracture networks depicted in the cross-section are schematic and reflect only zones where fracturing was directly characterized during site investigations.

Fig. 1 - Sezione stratigrafica concettuale dell'area di studio che illustra le principali unità idrostratigrafiche. Le variazioni nello spessore degli strati, le interruzioni e l'interdigitazione dei livelli evidenziano il complesso ambiente deposizionale che controlla il flusso idrico sotterraneo. I piezometri rappresentati lungo la sezione indicano gli intervalli filtrati e i livelli piezometrici utilizzati per la calibrazione del modello. Il reticolo di fratturazione rappresentato nella sezione è schematico e riflette esclusivamente le zone in cui la fratturazione è stata direttamente osservata durante le indagini in sito.

Implementation of groundwater flow model

In this study, a numerical groundwater flow model has been developed using MODFLOW-USG Version 1 (Panday et al., 2013) that solves the three-dimensional groundwater flow equation on unstructured grids, enabling flexible spatial discretisation of complex hydrogeological domains. The model has been divided vertically into six layers, each identifying a specific hydrostratigraphic unit, as shown in Table 1 and Figure 2a.

Tab. 1 - Summary of the hydro-stratigraphic units identified in the study area. The table lists the main geological layers incorporated into the conceptual and numerical groundwater model, highlighting their lithological characteristics.

Tab. 1 - Sintesi delle unità idrostratigrafiche individuate nell'area di studio. La tabella riporta i principali livelli geologici utilizzati nel modello concettuale e numerico di flusso sotterraneo, descrivendone le caratteristiche litologiche.

Layer	Hydrostratigraphic unit
1	Alluvial deposits, mostly consisting of silts and sands
2	Upper pozzolanic deposits
3	Tuffaceous deposits, generally lithified but locally highly fractured
4	Paleosol layer
5	Lower pozzolanic deposits
6	Basaltic lavas with a variable degree of fracturing

The purpose of the model is to configure two hydraulic barriers to reclaim contaminated groundwater flowing in the fractured tuffaceous deposits (layer 3, intermediate aquifer) and in the pozzolanic and lava layers (layers 5 and 6, deep aquifer). Layers 1, 2 and 3 were considered as unconfined, while layers 4, 5 and 6 were treated as confined. The upper alluvial deposits (layers 1 and 2), which mainly host infiltration or perched water, are not the focus of the present study.

Although on a large-scale intermediate and deep aquifers are hydraulically separated by the paleosol layer (i.e., layer 4), pumping tests show the local absence or thinning of the paleosol layer, which can lead to leakage (i.e., drainage) from the intermediate to the underlying deep units. In the model, the areas where vertical flow may occur (Fig. 2a) are represented by increasing the vertical component of hydraulic conductivity (i.e., Kz) within layer 4.

Constant-head boundary conditions were applied at the northern and southern boundaries of model layers 3 and 5 (intermediate and deep aquifers, respectively) to reproduce the observed regional groundwater flow direction and measured hydraulic gradients. Recharge rates have been assigned to the model according to land cover type: higher values have been applied to vegetated areas, where greater infiltration is expected, whereas lower values have been set to paved areas, which limit vertical water flow. The recharge has been estimated using the Thornthwaite method (Thornthwaite, 1948), based on the available meteorological data, including precipitation and air temperature records, covering the period from 2019 to 2024. Accordingly, a recharge rate of 150 mm/yr was assigned to vegetated areas, while a value of 15 mm/yr was assigned to paved areas.

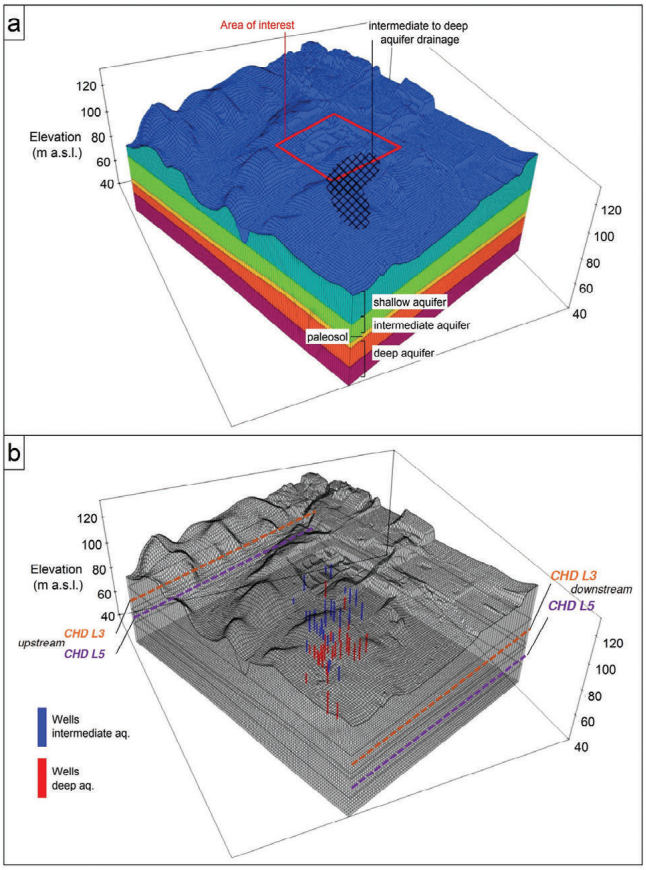

Fig. 2 - a) Three-dimensional representation of the numerical model domain showing the discretized topography and the stacked hydro-stratigraphic units used in the groundwater-flow model. The shallow, intermediate, and deep aquifers, together with the intervening paleosol layer, are highlighted, along with the designated area of interest and the zone of intermediate-to-deep aquifer drainage. (b) Spatial distribution of pumping wells included in the model, with blue symbols indicating wells screened within the intermediate aquifer and red symbols representing those completed in the deep aquifer. Spatial distribution of the constant-head boundary conditions assigned to model layers 3 (orange) and 5 (purple).

Fig. 2 - a) Rappresentazione tridimensionale del dominio del modello numerico che mostra la topografia discretizzata e le unità idrostratigrafiche sovrapposte utilizzate nelle simulazioni di flusso sotterraneo. Sono evidenziati l'acquifero superficiale, intermedio e profondo, insieme all'orizzonte di paleosuolo, all'area di interesse e alla zona di drenaggio dall'acquifero intermedio verso quello profondo. (b) Distribuzione spaziale dei pozzi di emungimento considerati nel modello, in blu i pozzi filtrati nell'acquifero intermedio in rosso quelli nei livelli profondi. Distribuzione spaziale delle condizioni al contorno di carico idraulico costante applicate ai layer 3 (arancione) e 5 (viola).

To assimilate the information from 13 pumping tests, a transient model with 41 stress periods was set up. The first stress period is steady-state and represents the undisturbed hydraulic conditions, serving as the initial condition for all subsequent transient simulations. The subsequent 40 transient stress periods simulate the pumping tests, performed on both intermediate and deep wells (Figure 2b), where observed drawdowns were used to facilitate estimation of storage parameters. The temporal configuration of these stress periods is summarized in the following Table 2.

The temporal structure of the stress periods was designed to reflect the sequence and duration of the pumping tests conducted at the site. Each pumping test comprises an active

Tab. 2 - Temporal discretization adopted in the groundwater-flow model: the table summarizes the sequence of stress periods used to simulate both steady-state and transient conditions. The initial stress period represents the calibrated steady-state groundwater levels for the intermediate and deep aquifers. Subsequent stress periods correspond to individual pumping test; each applied to either the intermediate or deep aquifer depending on well completion depth.

Tab. 2 - Discretizzazione temporale adottata nel modello di flusso sotterraneo: la tabella riassume la successione dei periodi di stress utilizzati per simulare condizioni stazionarie e transitorie. Il primo periodo rappresenta i livelli idrici stazionari per gli acquiferi intermedio e profondo. I periodi successivi corrispondono ai singoli test di pompaggio, applicati rispettivamente all'acquifero intermedio o profondo in funzione della profondità dei pozzi.

Stress Periods	Stresses	Investigated Aquifer
1	Steady-state levels	Intermediate, Deep
2–3	Pumping Test 1	Intermediate
4	Pumping Test 2 and 3	Intermediate
5	Pumping Test 4, 5, 6	Intermediate
6–11	Pumping Test 7	Deep
12–15	Pumping Test 8	Deep
16–19	Pumping Test 9	Deep
20–24	Pumping Test 10	Deep
25-29	Pumping Test 11	Deep
30–35	Pumping Test 12	Deep
36–41	Pumping Test 13	Deep

pumping phase followed by a recovery phase, and these were discretized into one or more stress periods depending on test complexity and duration. Shorter tests with straightforward hydraulic responses (e.g., Pumping Tests 2–6 in the intermediate aquifer) were assigned to single stress periods. Longer deep-aquifer tests (e.g., Pumping Tests 7–13), which involved extended pumping phases and prolonged recoveries, were discretized into multiple sequential stress periods to adequately resolve the time-varying hydraulic dynamics. This strategy balances temporal resolution against computational tractability.

The ENSI approach

ENSI is a derivative-free, ensemble-based inversion technique that enables the calibration of highly parameterized models by operating within a reduced-dimensional subspace derived from an ensemble of stochastic prior realizations, while applying regularization to constrain parameter estimation and ensure physically plausible solutions (Doherty, 2021).

Unlike traditional calibration approaches that adjust parameters individually or rely on full sensitivity matrices, can become computationally prohibitive or unstable for complex numerical models, ENSI focuses on a restricted set of super-parameters (i.e., low-dimensional combinations of native model parameters that capture the principal directions of model sensitivity), avoiding full Jacobian construction (Tonkin & Doherty, 2005; Doherty, 2021). In this framework, the inversion produces a calibrated parameter set that reflects the reduction of uncertainty along data-informed directions, while the ensemble structure preserves prior variability where the system remains poorly constrained.

The ENSI approach is applied according to the procedure and equations described below, where bold lower-case symbols denote vectors and bold upper-case symbols denote matrices. This notation is used to distinguish native parameter vectors, ensemble matrices, covariance matrices, and observation vectors.

1. *Generation of a prior ensemble*: a prior ensemble of N_e realizations of the parameter vector m is generated:

$$M_{prior} = \left[m^{(1)}, m^{(2)}, ..., m^{(N_e)} \right] \quad 1)$$

where each $m^{(i)}$ represents a plausible set of parameter values reflecting spatial variability (e.g., hydraulic conductivity, specific yield, specific storage).

2. *Definition of the ensemble-based inversion subspace*: instead of performing a full inversion in the native parameter space, ENSI restricts the solution to the subspace defined by the deviations of ensemble members from the mean:

$$X = \left[m^{(1)} - \bar{m}, m^{(2)} - \bar{m}, ..., m^{(N_e)} - \bar{m} \right] \quad 2)$$

where the vector $\bar{m}$ is the ensemble mean and $m^{(1)} - \bar{m}$ denotes the deviation of each ensemble member from the mean vector. The super-parameters, s, are linear combinations of the ensemble deviations:

$$m = \bar{m} + Xs \quad 3)$$

where s is the vector of realization factors, or super-parameters. This reduces the dimensionality of the inversion from the full parameter space to the number of ensemble members N_e.

3. *Regularized inversion in ensemble space:* given the vector of observations d^{obs} and the corresponding simulated outputs d^{sim}, the super-parameters are adjusted by minimizing the following regularized weighted least-squares objective function:

$$\Phi_{(s)} = \| W_d \left[d^{obs} - d^{sim}(s) \right] \|_2^2 + \lambda \| s - s_{prior} \|_2^2 \quad 4)$$

where W_d is the observation-weighting matrix, λ is the regularization parameter, and the squared Euclidean norm explicitly defines the weighted residual and regularization terms. The ENSI update can be expressed as:

$$s_{adj} = s_{prior} + C_{sf} C_{ff}^{-1} \left(d^{obs} - d^{sim} \right) \quad 5)$$

where C_{sf} is the cross-covariance matrix between the super-parameter ensemble and the simulated model-output ensemble, while C_{ff} is the auto-covariance matrix of the simulated model-output ensemble. These matrices are obtained directly from the prior ensemble simulations as sample covariance matrices. Let F be the matrix containing the simulated outputs for all prior realizations and let S be the corresponding matrix of prior super-parameter values. Defining S prime and F prime as the column-wise deviations from their respective

ensemble means, the sample covariance matrices are:

$$C_{sf} = \frac{1}{N_e - 1} S'(F')^T, C_{ff} = \frac{1}{N_e - 1} F'(F')^T \quad 6)$$

The ENSI method performs a single-pass linear update in the ensemble subspace: the super-parameters are adjusted once, and no iterative re-computation of C_{sf} or C_{ff} is required. In the implementation adopted here, these covariance matrices are computed once from the prior ensemble and are not updated at each optimization step. The optimization is thus reduced to a single matrix-vector operation, making the approach computationally efficient.

4. *Reconstruction of the optimized parameter fields:* once the inversion is completed in the ensemble space, the native parameter fields are reconstructed according to the following equation:

$$m_{adj} = \bar{m} + Xs_{adj} \quad 7)$$

producing geologically plausible distributions that reflect both the prior knowledge and the observational constraints.

Unlike ensemble-based methods such as the iterative Ensemble Smoother (iES; White, 2018) or Data-Space Inversion (DSI; Delottier et al., 2023), ENSI yields a single deterministic best-fit parameter set rather than a posterior ensemble of solutions. As a consequence, ENSI does not provide full characterization of parameter uncertainty by itself.

ENSI allows the contextual calibration of super-parameters and the so-called *"nonrealization parameters"*, which are individual parameters not statistically tied to others, such as boundary conditions or zoned recharge rates.

Calibration process with the ENSI approach

Calibration of the groundwater flow model has been addressed using the ENSI methodology, implemented through the PEST_HP (version 18) software suite (Doherty, 2024). A total of 1,986 field observations, comprising both hydraulic heads and drawdowns collected by automatic probes during the pumping tests, were provided as observations (Fig. 3c, d).

To capture the high spatial heterogeneity of specific parameters characterizing the investigated volcanic multi-aquifer system, a total number of 480 pilot points was distributed over the six model layers with a higher spatial density in the area of the industrial plant (Fig. 3a, b). Pilot points were used to estimate horizontal hydraulic conductivity (Kx, Ky), specific yield (Sy), and specific storage (Ss). Prior parameter distributions were derived from literature on volcanic aquifer systems (Custodio & Llamas, 1983; Civita & De Maio, 2000) and adjusted based on field evidence and expert knowledge. To better constrain the calibration of the hydraulic conductivity fields, the Kx and Ky values deduced from pumping tests at specific well and monitoring well locations were incorporated as pilot points and used to inform the parameter optimization process. In addition to these parameters, the estimation process also included constant head boundary conditions, recharge rates and the anisotropy ratio Kz/Kx; the latter was assumed as spatially uniform over the model domain but varied between layers.

Using the ENSI approach, multiple stochastic realizations of Kx, Ky, Sy, and Ss were generated across the six model layers, starting from pilot point distributions. The number of stochastic realizations was defined according to the role of each parameter group in the calibration process, the expected degree of spatial variability, the available field constraints, and the computational cost of the ENSI procedure. A larger ensemble was adopted for the hydraulic conductivity fields, with 180 realizations generated for Kx and Ky. This choice reflects the dominant influence of hydraulic conductivity on both the steady-state hydraulic-head distribution and the propagation of transient drawdowns, as well as the strong spatial heterogeneity expected in the volcanic deposits. Moreover, hydraulic conductivity was partly constrained by independent estimates derived from pumping tests, which provided additional support for representing its spatial variability in greater detail. A smaller ensemble, consisting of 100 realizations, was instead used for the storage parameters Sy and Ss. These parameters mainly affect the transient drawdown and recovery responses and are less directly constrained in space by the available observations. Therefore, a lower number of realizations was adopted to represent their prior variability while limiting the dimensionality of the ensemble subspace and the associated computational burden. The adopted ensemble sizes should thus be regarded as modelling choices aimed at balancing prior geological variability, parameter sensitivity, data support, and computational efficiency. Although no formal convergence analysis with respect to the number of ensemble members or alternative random realization sets was performed, the plausibility of the adopted ensemble configuration was evaluated a posteriori through calibration statistics, residual analysis, and comparison of optimized hydraulic conductivity values with independent pumping-test estimates.

Recharge rates, the anisotropy ratio (Kz/Kx), and boundary conditions were included in the ENSI framework as nonrealization parameters, with their uncertainty represented by constant standard deviations. For the realization parameters (Kx, Ky, Sy, Ss), uncertainty was expressed through covariance matrices associated with the stochastic fields. The resulting ensemble of stochastic realizations formed the basis for dimensionality reduction within ENSI.

The ENSI approach implicitly applies regularization by constraining the solution to the ensemble subspace. This integrated parameterization allowed the simultaneous calibration of spatially distributed and nonrealization parameters, preserving geological realism while maintaining computational efficiency.

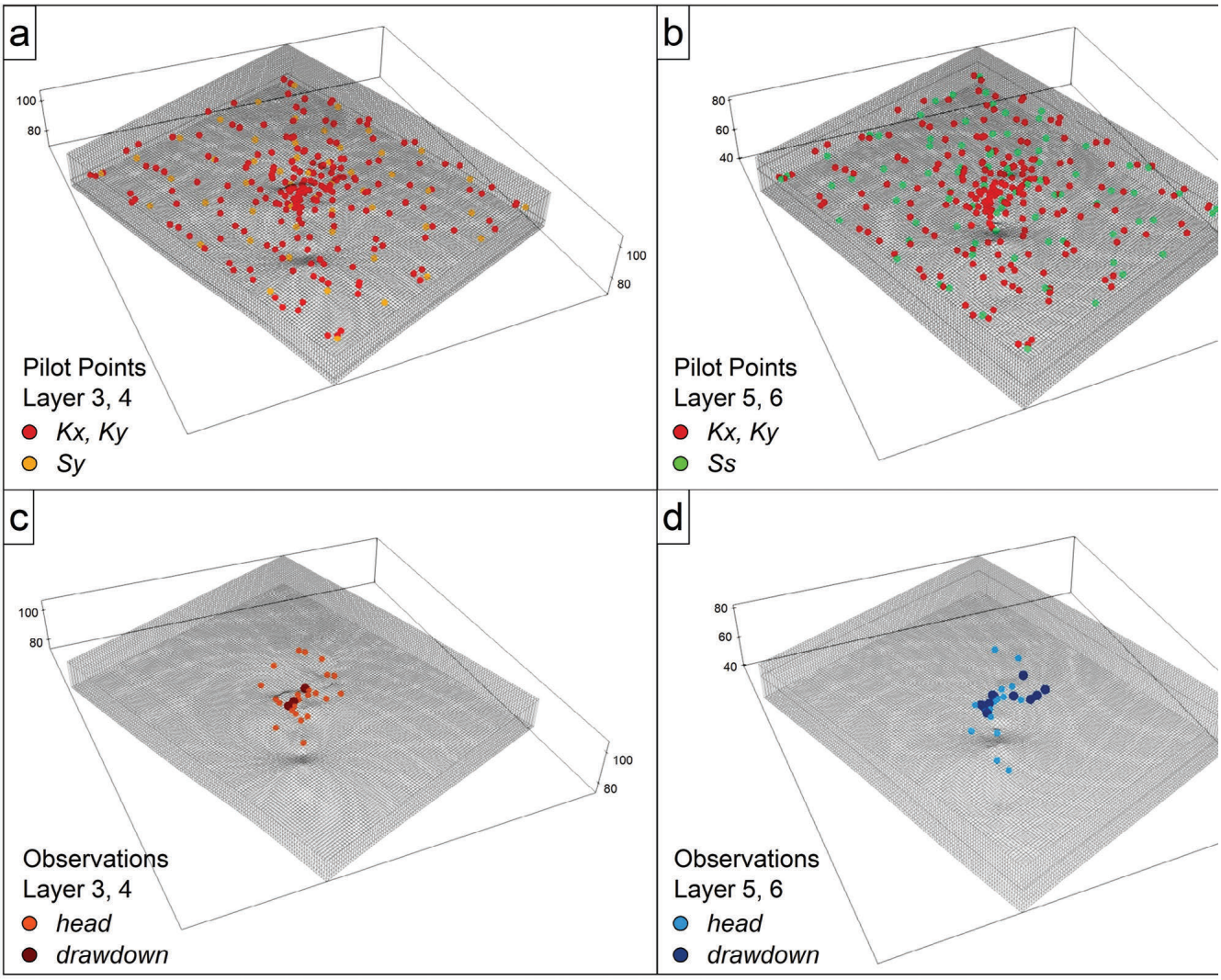

Fig. 3 - Spatial arrangement of pilot points and observational targets used for ENSI parameter estimation in the groundwater-flow model. (a) Distribution of pilot points assigned to the intermediate aquifer and paleosol layer (model layers 3–4), parameterized for horizontal hydraulic conductivity (Kx, Ky) and specific yield (Sy). (b) Distribution of pilot points assigned to the deep aquifer (model layers 5–6), parameterized for horizontal hydraulic conductivity (Kx, Ky) and specific storage (Ss). (c) Observation wells used to constrain head and drawdown responses in the intermediate aquifer. (d) Observation wells used to constrain head and drawdown responses in the deep aquifer.

Fig. 3 - Distribuzione dei pilot points e dei dati osservati utilizzati per la stima parametrica nel modello di flusso sotterraneo. (a) Distribuzione dei pilot points assegnati all'acquifero intermedio e all'orizzonte di paleosuolo (layer 3–4 del modello), parametrizzati per la conducibilità idraulica orizzontale (Kx, Ky) e la resa specifica (Sy). (b) Distribuzione dei pilot points assegnati all'acquifero profondo (layer 5–6), parametrizzati per la conducibilità idraulica orizzontale (Kx, Ky) e la compressibilità specifica (Ss). (c) Pozzi di osservazione utilizzati per vincolare i livelli piezometrici e gli abbassamenti nell'acquifero intermedio. (d) Pozzi di osservazione utilizzati per vincolare i livelli piezometrici e gli abbassamenti nell'acquifero profondo.

Results

ENSI calibration performance has been evaluated through quantitative metrics for both steady-state and transient conditions, together with the calibrated hydraulic parameter fields and their comparison against independent field-based estimates.

For the steady-state simulation (Stress Period 1), model performance has been assessed against measured hydraulic heads (Figure 4a), providing a mean absolute error of 0.09 m and a root mean square error (RMSE) of 0.47 m. When scaled to the full range of measured heads (16.43 m), these errors correspond to relative values below 3%, which can be considered well within acceptable limits for regional groundwater modeling. Overall, the residuals appeared symmetrically distributed around the 1:1 line in the calibration scatterplot, and their spatial distribution showed no significant clustering or bias. A tendency to underestimate deep aquifer levels is not concerning, given the very short observation range.

Considering the transient simulations, the comparison between observed and simulated drawdown during individual pumping tests (examples in Figure 4b) showed a generally good agreement and demonstrates the model's ability to: (i) reproduce the magnitude of maximum drawdown, (ii) capture the rate of drawdown development and its spatial attenuation with distance from the pumping well, and (iii) simulate the recovery dynamics, including partial recovery in wells subject to overlapping or sequential pumping events.

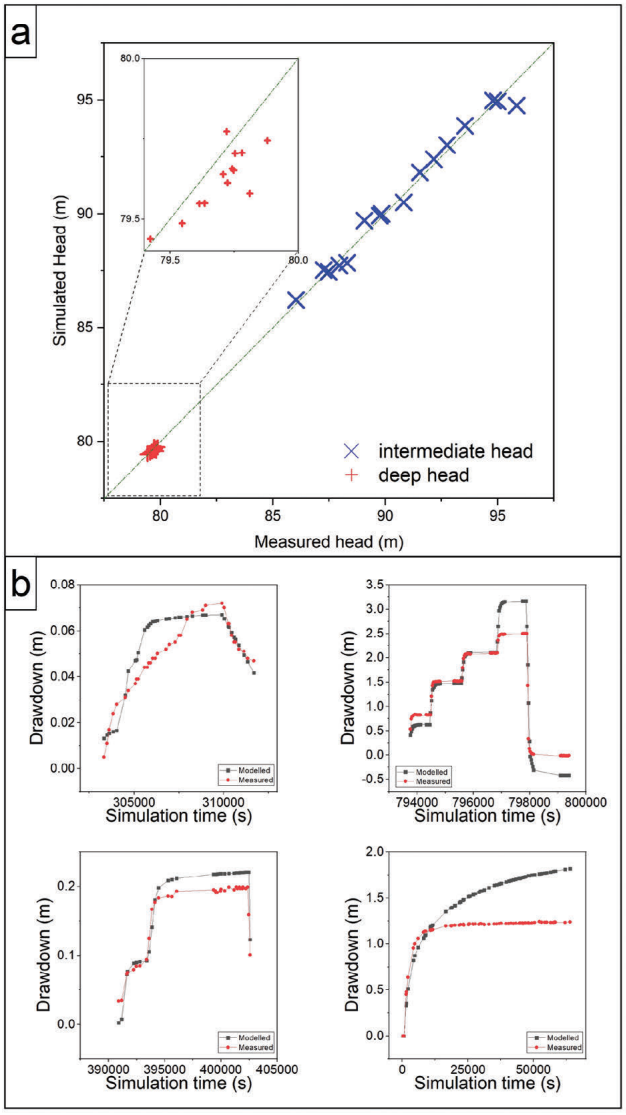

Fig. 4 - Model calibration results for steady-state and transient conditions. (a) Scatterplot comparing simulated and measured hydraulic heads for the first steady-state stress period. Blue symbols represent observations in the intermediate aquifer, while red symbols correspond to the deep aquifer. The alignment of points along the 1:1 line indicates the model's ability to reproduce the spatial distribution of observed hydraulic heads; the inset highlights the narrower range of deep-aquifer heads. (b) Representative examples of time series of transient drawdown history matching for selected monitoring wells across both aquifer systems (stress periods 2–41). Each panel plots the temporal evolution of simulated (black curve) versus observed (red curve) drawdown during individual pumping tests, spanning both the active pumping phase and the subsequent recovery.

Fig. 4 - Risultati della calibrazione del modello in condizioni stazionarie e transitorie. (a) Diagramma di dispersione tra livelli idrici simulati e misurati per il primo periodo di stress in condizioni stazionarie. I simboli blu rappresentano le osservazioni nell'acquifero intermedio, mentre i simboli rossi indicano l'acquifero profondo. La vicinanza dei punti alla linea 1:1 evidenzia la capacità del modello di riprodurre la distribuzione spaziale dei livelli osservati; il riquadro mostra nel dettaglio il range ristretto dei livelli dell'acquifero profondo. (b) Esempi rappresentativi del confronto tra andamento simulato e misurato degli abbassamenti durante i periodi di stress 2–41, relativi a diversi test di pompaggio selezionati in entrambi i corpi idrici sotterranei. Ogni pannello riporta l'evoluzione temporale dell'abbassamento simulato (curva nera) e osservato (curva rossa) durante le singole prove di pompaggio, includendo sia la fase di pompaggio attivo sia la successiva fase di recupero.

Discrepancies between observed and simulated drawdown curves were observed in a few locations, where residuals exceeded one meter. The largest discrepancies were mainly observed at pumping wells and are likely attributable to pumping-induced disturbances and associated non-linear head losses that are not explicitly represented in the model.

The satisfactory outcome of the optimization process is further supported by calibration statistics summarized in Figure 5. Statistical residuals calculated for each well showed root mean square errors typically within the centimetre range and mean residuals close to zero, indicating that both the timing and magnitude of drawdowns were effectively reproduced. The distribution of mean residuals is tightly clustered around zero, with limited spread and only a few moderate outliers, confirming the absence of systematic bias in the simulated drawdowns. Minimum and maximum residuals show broader variability, reflecting local mismatches at a subset of wells, while the presence of a few high positive outliers in the maximum residuals aligns with the locations where discrepancies exceeded one meter. The boxplots of absolute mean residuals and RMSE further corroborate the generally good model performance: both metrics remain low for most targets, with median values well below 0.5 m. The overall pattern suggests a calibration that is robust across most of the domain, with only isolated areas exhibiting larger deviations. Major mismatches may be attributed to site-specific nonlinear head losses or uncertainties in the field-testing conditions, such as unaccounted well inefficiencies or localized heterogeneities not resolved in the model grid. Nonetheless, the overall ability of the model to reproduce drawdowns over such a large and heterogeneous dataset validates the robustness of the ENSI approach.

The parameter fields resulting from the calibration process are geologically consistent and aligned with the site's conceptual model (Fig. 6). For instance, the horizontal hydraulic conductivity in layer 3 (i.e., tuffaceous deposits) has an average value of 2.6×10^{-4} m/s, while the average specific yield is 1.2×10^{-2}. Layer 4 (i.e., paleosol layer), which acts as an aquitard, exhibits much lower conductivity values (average value equal to 4.4×10^{-8} m/s) and a specific yield of 7.0×10^{-5}. In contrast, layer 5 (i.e., lower pozzolanic deposits) and layer 6 (i.e., basaltic lavas) show higher hydraulic conductivity values, with average values of 1.6×10^{-3} m/s and 1.1×10^{-3} m/s, respectively. These parameters reflect the stratigraphic variability of the volcanic deposits and are in line with known hydrogeological conditions. Notably, areas exhibiting relatively high Kx, Ky and Kz values in layer 4 in the western portion of the study area correspond well to the zones of drainage from the intermediate to the deep aquifer identified during pumping tests.

To validate the plausibility of the calibrated hydraulic conductivity fields, model-optimized parameter values were compared with independent estimates obtained from field-based pumping tests (Figure 7). The comparison revealed a high degree of correlation, often within the same order of magnitude, across both intermediate and deep aquifer

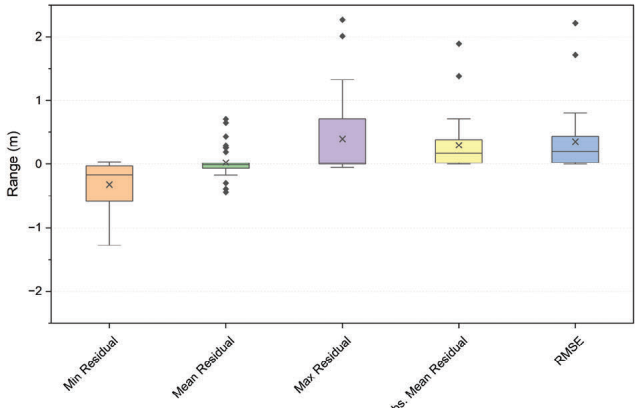

Fig. 5 - Boxplots summarizing the statistical distribution of residuals between simulated and observed drawdowns. The figure presents minimum, mean, and maximum residuals, absolute mean residuals, and root mean square error (RMSE) computed across all pumping-test observations. Boxes represent the interquartile range, whiskers indicate the full spread of non-outlier values, and markers denote outliers and group means. These statistics provide a comprehensive assessment of model predictive performance and highlight the variability in the agreement between simulated and measured drawdown responses.

Fig. 5 - Diagrammi a scatola che riassumono la distribuzione statistica dei residui tra abbassamenti simulati e osservati. La figura mostra i residui minimi, medi e massimi, il valore assoluto del residuo medio e la radice dell'errore quadratico medio (RMSE) calcolati sull'insieme delle osservazioni dei test di pompaggio. Le scatole rappresentano l'intervallo interquartile, i baffi indicano l'estensione dei valori non anomali e i simboli evidenziano outlier e valori medi. Queste statistiche permettono di valutare in modo completo la qualità predittiva del modello e la variabilità dell'accordo tra abbassamenti simulati e misurati.

zones. This agreement further supports the reliability of the calibration results and the ability of ENSI to generate geologically and hydraulically consistent parameter fields.

Among the nonrealization parameters, recharge was differentiated between vegetated (112 mm/year) and paved areas (2 mm/year), consistent with expected infiltration patterns. Anisotropy ratios Kz/Kx were estimated for each hydrostratigraphic layer, with values ranging from 0.06 to 0.46, depending on lithology and depth. Constant-head boundary conditions were calibrated for the upstream and downstream edges of the model in layers 3 and 5, reflecting the regional hydraulic gradient and controlling the lateral inflow and outflow.

Discussion

In this study, all available observations (i.e., steady-state hydraulic heads, transient drawdowns, and multi-aquifer monitoring data) were assimilated simultaneously within a unified calibration framework. Rather than partitioning or filtering the dataset, all 1,986 measurements were jointly used, ensuring that both short-term hydraulic responses and long-term system behavior were honored. Calibrating across the full suite of stress periods yielded parameter estimates that are potentially representative of a wide range of hydrological conditions, thereby strengthening predictive simulations and scenario analyses.

The representation of complex patterns of heterogeneity associated with hydraulic property of a volcanic multi-aquifer system, together with the high dimensionality of the inverse

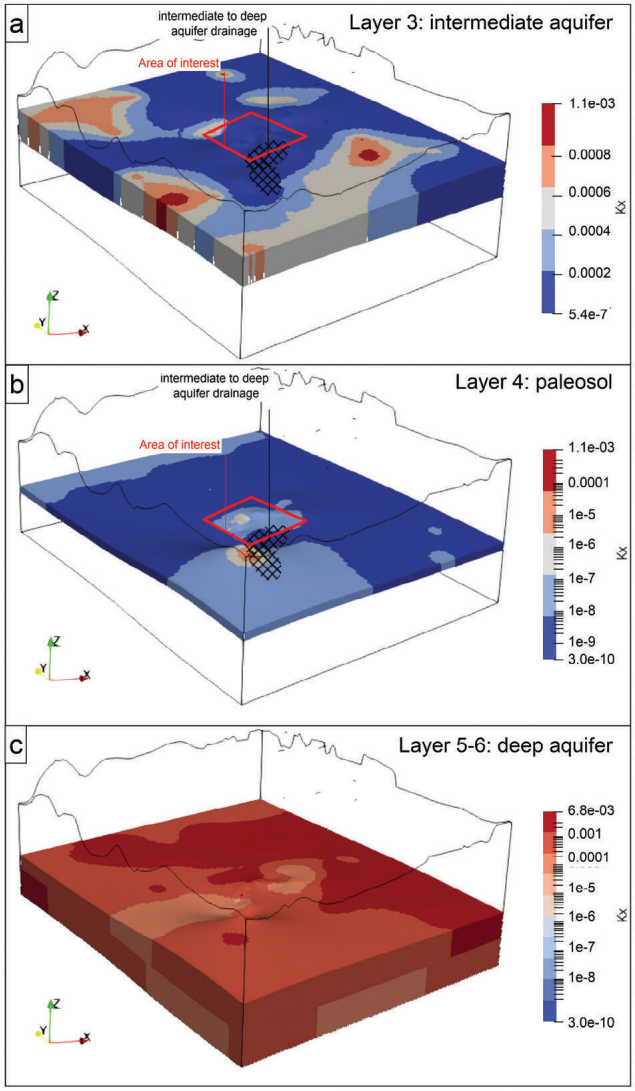

Fig. 6 - Estimated hydraulic conductivity fields for the calibrated groundwater-flow model. (a) Horizontal hydraulic conductivity (Kx) distribution for the intermediate aquifer (Layer 3), showing spatial heterogeneity linked to sedimentary facies variability and zones of enhanced permeability. (b) Hydraulic conductivity field for the paleosol layer (Layer 4), characterized by generally low K values with localized higher-permeability zones. (c) Hydraulic conductivity distribution for the deep aquifer system (Layers 5–6), where broader regions of elevated K reflect the more transmissive volcanic deposits. In all panels, the area of interest and the inferred pathway of intermediate-to-deep aquifer drainage are highlighted to support interpretation of flow connectivity across hydrostratigraphic units.

Fig. 6 - Campi di conducibilità idraulica stimati per il modello di flusso sotterraneo calibrato. (a) Distribuzione della conducibilità idraulica orizzontale (Kx) nell'acquifero intermedio (layer 3), che evidenzia l'eterogeneità spaziale legata alla variabilità delle facies sedimentarie e alle zone a maggiore permeabilità. (b) Campo di conducibilità idraulica nel livello di paleosuolo (layer 4), caratterizzato da valori generalmente bassi con alcune aree a permeabilità più elevata. (c) Distribuzione della conducibilità idraulica nell'acquifero profondo (layer 5–6), dove ampie zone con valori più alti riflettono la maggiore trasmissività dei depositi vulcanici. In tutti i pannelli sono riportate l'area di interesse e la via preferenziale di drenaggio dall'acquifero intermedio verso quello profondo, al fine di supportare l'interpretazione della connettività idraulica tra le unità idrostratigrafiche.

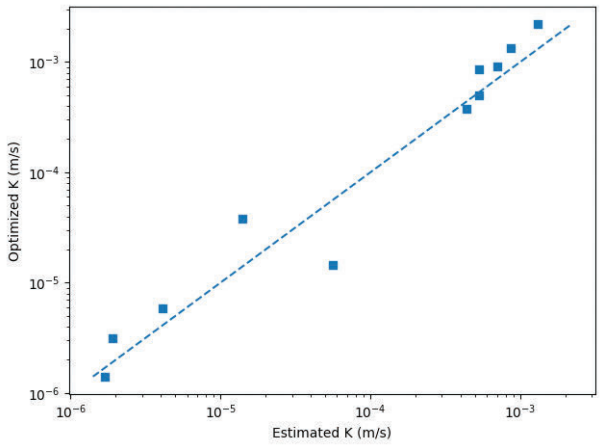

Fig. 7 - Comparison between hydraulic conductivity values estimated from pumping tests and those optimized through the ENSI-based calibration procedure. The scatterplot compares independently estimated K values with model-optimized K values. The strong correlation indicates that the ENSI optimization framework reliably reproduces field-derived transmissivity conditions, supporting the internal consistency and robustness of the calibrated hydraulic parameter set.

Fig. 7 - Confronto tra i valori di conducibilità idraulica stimati dai test di pompaggio e quelli ottimizzati tramite la procedura di calibrazione ENSI. Il diagramma di dispersione mette a confronto i valori di K stimati sperimentalmente con quelli ottimizzati dal modello. L'elevata correlazione evidenzia la capacità del metodo ENSI di riprodurre coerentemente le condizioni osservate in campo, confermando l'affidabilità del set di parametri idraulici calibrati.

problem, required an advanced model calibration strategy. Unlike the standard GLM-based inversion method, ENSI achieves efficiencies in model calibration by working in a reduced parameter space that is defined by realizations of prior parameter probability distribution, ensuring physically plausible parameter fields.

By drastically reducing problem dimensionality, ENSI gains numerical benefits and operates a rapid decrease of the objective function (Φ), which quantifies the least-squares misfit between observed and simulated values. The convergence of Φ was smooth, stable, and, based on the authors' experience, markedly faster than with conventional methods such as PEST, even equipped with SVD. Convergence trends were evaluated separately for hydraulic heads in the intermediate and deep aquifers, as well as for transient drawdowns from pumping tests. In all cases, residuals decreased progressively across iterations, confirming the robustness of the dimensionality-reduction framework.

Using regularized inversion, ENSI yielded spatial distributions of the estimated parameters (i.e., Kx, Kz, Sy and Ss) that proved geologically plausible and consistent with the real hydrogeological system. This aligns with previous findings on the effectiveness of Tikhonov regularization in preserving geological realism (Carrera et al., 2005). The calibrated model also reproduces key hydrogeological features of the system, including complex vertical hydraulic interactions, leakage pathways, and locally developed low-permeability or dry zones in downgradient sectors of the intermediate aquifer.

Model-data agreement and calibration statistics further support the performance of the ENSI-based optimization process. Under steady-state conditions, mean residuals remained below 10 cm and the RMSE reached 47 cm; these values are commensurate with the target level of fit and are nonetheless remarkable given the structural complexity of the system. Transient simulations, involving over 1,900 head and drawdown observations, provided similar results, with drawdown residuals within centimetres in most monitoring wells. Time-series comparisons demonstrate that the model reproduces both the magnitude and timing of drawdowns across stress conditions and aquifer layers.

A major advantage of ENSI is that it offers a substantial reduction of the computational costs associated with history-matching. Compared to conventional calibration approaches requiring thousands of forward model runs, ENSI achieved convergence with orders of magnitude fewer simulations, significantly improving the tractability of the inverse problem. This efficiency made it possible to retain a high-resolution pilot-point parameterization (480 pilot points) and to assimilate the full observational dataset without the need for manual dimensionality reduction. This feature is particularly valuable in applied contexts where computational resources and time constraints are critical.

The calibration performance achieved in this application is consistent with findings reported for ensemble-based and regularised inversion methods applied to complex multi-aquifer systems. Hayley et al. (2019) demonstrated significant reductions in computational effort using the iterative Ensemble Smoother in a multi-layer aquifer setting. The geological plausibility of regularised inversion results was validated by Carrera et al. (2005), who showed that Tikhonov-regularised parameter fields reproduce observed spatial patterns without sacrificing calibration accuracy. The effectiveness of pilot-point parameterisation in capturing spatial heterogeneity was demonstrated by Doherty & Hunt (2010) and Fienen et al. (2009). Kitlasten et al. (2025) explicitly benchmarked ENSI and DSI in a complex alluvial aquifer, confirming that ensemble-space methods reduce forward model calls by orders of magnitude relative to GLM-based approaches, consistent with the computational savings reported in this study.

A fundamental limitation of the ENSI approach is that it yields a single best-fit parameter realization and does not explicitly quantify parameter uncertainty. The resulting spatial distributions of hydraulic conductivity, while geologically consistent and supported by available data, should therefore be interpreted as deterministic estimates rather than probabilistic outcomes. Full uncertainty characterization requires post-calibration analyses or alternative ensemble-based frameworks.

In this context, methods such as iES (White, 2018) or DSI (Delottier et al., 2023) may be used to extend the analysis toward a probabilistic framework. Similarly, null-space Monte Carlo approaches (Doherty, 2025) or related techniques can be employed to explore parameter uncertainty around the calibrated solution. Nonetheless, ENSI provides a robust and efficient foundation for such subsequent analyses, allowing

uncertainty quantification to be scaled according to the needs of the project.

Conclusions

The results presented in this study demonstrate the practical effectiveness of ENSI as a calibration tool for complex, high-dimensional volcanic multi-aquifer systems. The adopted framework enabled the simultaneous assimilation of steady-state hydraulic heads, transient drawdowns, and multi-aquifer monitoring data within a unified calibration process, allowing both short-term hydraulic responses and long-term groundwater system behavior to be consistently represented.

The high degree of spatial heterogeneity characterizing the investigated volcanic aquifer system, together with the large number of adjustable parameters, made the inverse problem particularly challenging for conventional GLM-based optimization approaches, which proved computationally impractical. By reducing the dimensionality of the parameter space through stochastic ensemble realizations, ENSI enabled the estimation of spatially distributed material properties (hydraulic conductivity and storage of several layers) and boundary conditions, while maintaining geological consistency and physically plausible solutions.

The calibrated model successfully reproduces both steady-state groundwater levels and transient drawdown responses associated with 13 pumping tests distributed across 41 stress periods. Model–data agreement demonstrated the capability of the proposed approach to reproduce the magnitude and temporal evolution of drawdowns, including recovery dynamics and complex inter-aquifer hydraulic interactions. Model performance metrics indicate a good agreement between simulated and observed data across the domain, highlighting the method's accuracy and reliability.

A major advantage of ENSI lies in its computational efficiency. Compared with traditional highly parameterized inversion approaches requiring thousands of forward simulations, ENSI achieved convergence with orders of magnitude fewer model runs. This computational advantage allowed the retention of a dense pilot-point parameterization and the assimilation of the complete observational dataset without the need for manual dimensionality reduction, substantially improving the tractability of the calibration process in a real-world hydrogeological application.

At the same time, an important methodological limitation must be explicitly acknowledged. ENSI yields a single deterministic best-fit parameter realization and does not provide a probabilistic characterization of parameter uncertainty. The calibrated parameter fields should therefore be interpreted as optimal estimates conditioned on the available observations rather than unique representations of the real hydrogeological system. Additional post-calibration analyses are required to quantify uncertainty and evaluate the range of parameter combinations compatible with the observed data.

Nevertheless, the calibrated solution obtained through ENSI provides a robust and geologically realistic basis for subsequent uncertainty quantification workflows, including iterative ensemble smoothers, null-space Monte Carlo analyses, and other ensemble-based probabilistic approaches. The combination of computational efficiency, stability in highly parameterized inverse problems, and adherence to geological realism makes ENSI a valuable tool for decision-support groundwater modelling in heterogeneous multi-aquifer systems.

Competing interest

The authors declare no competing interest.

AI use declaration statement

The authors used Claude AI during the writing process to improve readability and grammar in some parts of the paper.

Author contributions

Collection of data, Mattia De Caro, Licia Pollicino; data processing, Mattia De Caro, Licia Pollicino; interpretation of results, Mattia De Caro, Licia Pollicino, Giovanni Formentin; writing-original draft preparation, Mattia De Caro, Licia Pollicino; writing-review and editing, Mattia De Caro, Licia Pollicino, Giovanni Formentin; visualization, Giovanni Formentin; supervision, Giovanni Formentin. All authors have read and agreed to the final version of the manuscript.

Additional information

DOI: https://doi.org/10.7343/as-2026-959

REFERENCES

Anderson, M. P., Woessner, W. W., & Hunt, R. J. (2015). Applied Groundwater Modeling: Simulation of Flow and Advective Transport (2nd ed.). Elsevier / Academic Press. ISBN 978 0 12 058103 0

Carrera, J., Alcolea, A., Medina, A., Hidalgo, J., & Slooten, L. J. (2005). Inverse problem in hydrogeology. Hydrogeology Journal, 13(1), 206–222. https://doi.org/10.1007/s10040-004-0404-7

Chen, Y., & Oliver, D. S. (2013). Levenberg–Marquardt forms of the iterative ensemble smoother for efficient history matching and uncertainty quantification. Computational Geosciences, 17, 689–703. https://doi.org/10.1007/s10596-013-9351-z

Civita, M., & De Maio, M. (2000). Vulnerability assessment of hydrogeological systems. Pitagora Editrice, Bologna.

Delottier, H., Doherty, J., & Brunner, P. (2023). Data space inversion for efficient uncertainty quantification using an integrated surface and sub-surface hydrologic model. Geoscientific Model Development, 16(14), 4213–4231. https://doi.org/10.5194/gmd-16-4213-2023

Doherty, J. (2003). Groundwater model calibration using pilot points and regularization. Ground Water, 41(2), 170–177. https://doi.org/10.1111/j.1745-6584.2003.tb02580.x

Doherty, J. (2021). ENSI: Ensemble-Space Inversion for Efficient Calibration of Highly Parameterized Models. Watermark Numerical Computing

Doherty, J. (2024). PEST_HP: PEST for highly-parallelized computing environments. Brisbane, Australia: Watermark Numerical Computing. Available online at: https:// www.pesthomepage.org

Doherty, J. (2025). Calibration and uncertainty analysis for complex environmental models. Watermark Numerical Computing, Brisbane

Doherty, J., & Hunt, R. J. (2010). Approaches to Highly Parameterized Inversion: A Guide to Using PEST for Groundwater-Model Calibration. U.S. Geological Survey Scientific Investigations Report 2010–5169. DOI: 10.3133/sir20105169

Fienen, M. N., Muffels, C. T., & Hunt, R. J. (2009). On constraining pilot point calibration with regularization in PEST. Ground Water, 47(6), 835–844. DOI: 10.1111/j.1745-6584.2009.00635.x

Hayley, K., Valenza, A., White, E., Hutchison, B., & Schumacher, J. (2019). Application of the Iterative Ensemble Smoother Method and Cloud Computing: A Groundwater Modeling Case Study. Water, 11(8), 1649. https://doi.org/10.3390/w11081649

Kitlasten, W., Moore, C., & Doherty, J. (2025). Exploring the use of new data assimilation technologies to map groundwater quality vulnerability in a large alluvial aquifer. Front. Earth Sci. 13:1609778. doi: 10.3389/feart.2025.160977

Lima, M. M., Emerick, A. A., & Ortiz, C. E. P. (2020). Data-space inversion with ensemble smoother. Comput. Geosci., 24, 1179–1200. doi:10.1007/s10596- 020-09933-w

Liu, D., Rao, X., Zhao, H., Xu, Y.-F., & Gong, R.-X. (2021). An improved data space inversion method to predict reservoir state fields via observed production data. Petroleum Sci. 18, 1127–1142. doi:10.1016/j.petsci.2021.07.008

Mariethoz, G., Renard, P., & Straubhaar, J. (2010). The Direct Sampling method to perform multiple-point geostatistical simulations. Water Resources Research, 46(11), W11536. https://doi.org/10.1029/2008WR007621

Moore, C., & Doherty, J.E., 2006. The cost of uniqueness in groundwater model calibration. Adv. Water Resour. 29, 605–623. doi: 10.1016/j.advwatres.20 05.07.0 03

Panday, S., Langevin, C. D., Niswonger, R. G., Ibaraki, M., & Hughes, J. D. (2013). MODFLOW–USG Version 1: An unstructured grid version of MODFLOW for simulating groundwater flow. US Geological Survey Techniques and Methods 6–A45

Sun, W., & Durlofsky, L. J. (2017). A new data-space inversion procedure for efficient uncertainty quantification in subsurface flow problems. Mathematical Geosciences, 49(6), 679–715

Thornthwaite, C. W. (1948). An approach toward a rational classification of climate. Geographical Review, 38(1), 55–94.

Tonkin, M. J., & Doherty, J. (2009). Calibration-constrained Monte Carlo analysis of highly parameterized models using subspace techniques. Water Resources Research, 45(12), W00B10. https://doi.org/10.1029/2007WR006678

Tonkin, M.J., & Doherty, J. (2005). A hybrid regularized inversion methodology for highly parameterized environmental models. Water Resources Research, 41, W10412

White, J. T. (2018). A model-independent iterative ensemble smoother for efficient history-matching and uncertainty quantification in very high dimensions. Environmental Modelling and Software, 109, 191–201. https://doi.org/10.1016/j.envsoft.2018.06.009